Article

Supercoiling Structure-Based Design of a Trimeric Coiled-Coil Peptide with High Potency against HIV-1 and Human β-Coronavirus Infection

Chao Wang,[#] Shuai Xia,[#] Xinling Wang,[#] Yue Li, Huan Wang, Rong Xiang, Qinwen Jiang, Qiaoshuai Lan, Ruiying Liang, Qing Li, Shanshan Huo, Lu Lu, Qian Wang,* Fei Yu,* Keliang Liu,* and Shibo Jiang*

Cite This: https://doi.org/10.1021/acs.jmedchem.1c00258

Read Online

ACCESS | Metrics & More | Article Recommendations | Supporting Information

ABSTRACT: Hexameric structure formation through packing of three C-terminal helices and an N-terminal trimeric coiled-coil core has been proposed as a general mechanism of class I enveloped virus entry. In this process, the C-terminal helical repeat (HR2) region of viral membrane fusion proteins becomes transiently exposed and accessible to N-terminal helical repeat (HR1) trimer-based fusion inhibitors. Herein, we describe a mimetic of the HIV-1 gp41 HR1 trimer, N3G, as a promising therapeutic against HIV-1 infection. Surprisingly, we found that in addition to protection against HIV-1 infection, N3G was also highly effective in inhibiting infection of human β-coronaviruses, including MERS-CoV, HCoV-OC43, and SARS-CoV-2, possibly by binding the HR2 region in the spike protein of β-coronaviruses to block their hexameric structure formation. These studies demonstrate the potential utility of anti-HIV-1 HR1 peptides in inhibiting human β-coronavirus infection. Moreover, this strategy could be extended to the design of broad-spectrum antivirals based on the supercoiling structure of peptides.

EC$_{50}$ (HIV-1) = 0.01 μM
EC$_{50}$ (MERS-CoV) = 0.46 μM
EC$_{50}$ (OC43) = 1.26 μM
EC$_{50}$ (SARS-CoV-2) = 3.14 μM
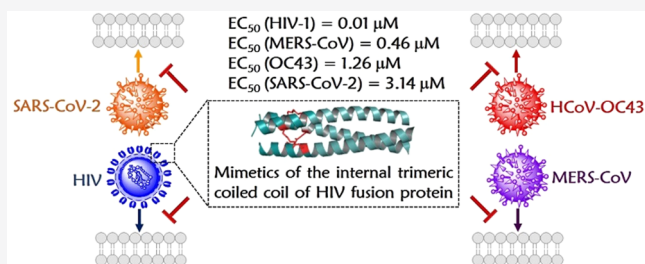
INTRODUCTION

A decade after the outbreak of severe acute respiratory syndrome coronavirus (SARS-CoV), Middle East respiratory syndrome coronavirus (MERS-CoV) first emerged in the Middle East in 2012, and as of November 2019, 2494 laboratory-confirmed cases of infection with this virus, including 858 deaths, had been reported to the World Health Organization.[1] Since December 2019, severe acute respiratory syndrome coronavirus 2 (SARS-CoV-2) has rapidly spread worldwide to become the third coronavirus posing a serious threat to global public health.[2] In addition to these highly pathogenic human coronaviruses (HCoVs), some low-pathogenicity coronaviruses, including HCoV-OC43, are also pandemic in humans and even cause fatal diseases in children, the elderly, and patients with chronic conditions.[3] Consequently, it is imperative to develop effective therapeutics and prophylactics against coronavirus infection.

Coronavirus spike (S) proteins are classified as structurally defined class I viral fusion glycoproteins that utilize a mechanism similar to that of other class I enveloped viruses, such as HIV-1 and Ebola virus, for membrane fusion.[4,5] A hallmark of this type of viral fusion glycoprotein is the formation of a six-helix bundle (6-HB) fusion core between the central N-terminal heptad repeat [NHR, also named heptad repeat 1 (HR1)] trimeric coiled coil and three copies of the antiparallel C-terminal heptad repeat [CHR, also named heptad repeat 2 (HR2)] of the membrane fusion subunit, which is a critical prelude to the coalescence of viral and cell membranes (Figure 1A).[6−8] Prior to the assembly of highly stable helical bundles, the CHR (HR2) and trimeric NHR (HR1) core become transiently exposed so that both units are accessible to fusion inhibitors.[9,10]

Mimicry of the HR1 helical trimers via coiled-coil stabilization methodology would allow for the construction of scaffolds targeting the HR2 region and thus open up an important area for the discovery of antiviral therapeutics.[11,12] Strategies for recapitulating the bioactive tertiary structure of HR1-based peptides include fusion of HR1 segments to auxiliary protein domains,[13−15] covalent stabilization,[16−18] and protein engineering according to the rule of thumb for trimeric coiled-coil nucleation.[19] HIV-1 gp41 NHR trimer mimetics are arguably the most typical example of such dominant-negative inhibitors that can block HIV-1 entry at nanomolar
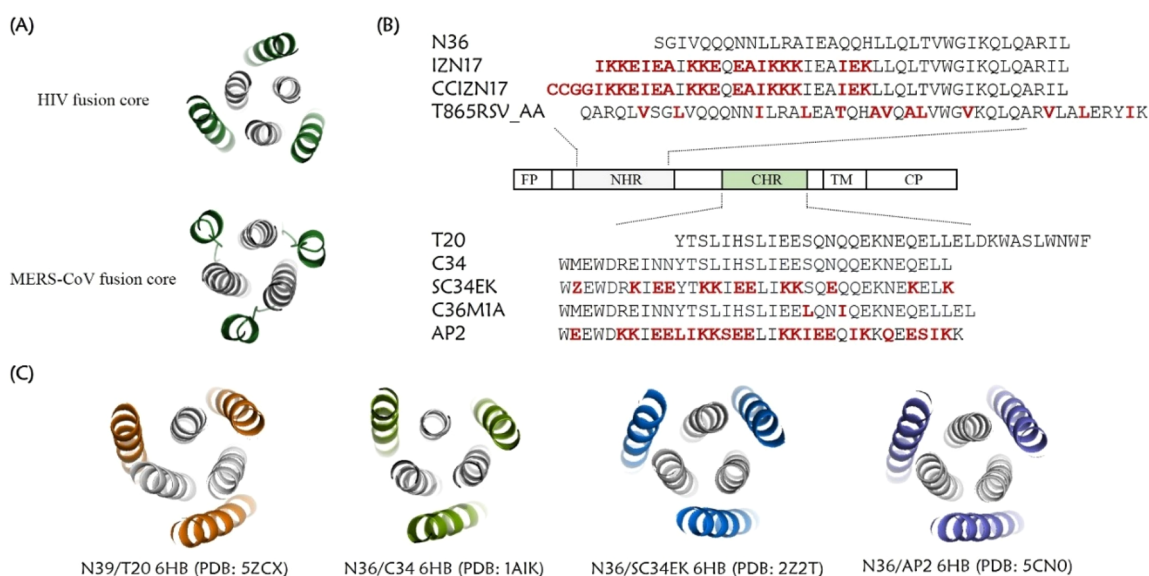
Figure 1. Postfusion structure models and schematic illustration of the HIV-1 gp41 protein. (A) Top view of the HIV-1 6-HB (PDB entry 1AIK) and MERS-CoV 6-HB (PDB entry 4NJL), in which the HR1 trimers and HR2 segments are colored gray and forest, respectively. (B) Sequences of HIV-1 gp41 HR1- or HR2-derived peptides. C34, T20, and N36 are native sequences based on HIV-1$_{HXB2}$ Env sequences. Mutated residues in peptide fusion inhibitor design are colored red. (C) Crystal structure of the T20/N39-, C34/N36-, SC34EK/N36-, and AP2/N36-based six-helical bundle. HIV-1 HR1 helical trimers are colored gray, and T20, C34, SC34EK, and AP2 are colored orange, split pea, blue, and violet, respectively.
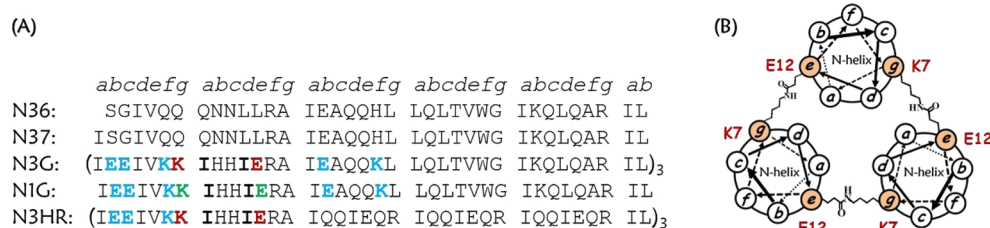

Figure 2. Design of helical trimers based on the HIV-1 6-HB model. (A) Primary sequence of our designed N3G and (B) its helical wheel diagram. The intramolecular E−K salt bridges are colored blue. The interhelical i to i' + 5 ionic interactions are colored green. Isopeptide bonds are formed between Lys7 at the g position on one strand per trimer and Glu12 at the e position on another strand (red). These peptides have an acetyl group at the N-terminus and a carboxyamide at the C-terminus.

concentrations. Interestingly, sequence−structure−activity analysis shows that these constructs allow a high permissibility in the primary structure of each helix as long as the trimeric bundle is maintained (Figure 1B). The engineered HR1 trimer and the target HR2 helix, e.g., C34, retain the ability to form a stable heterologous 6-HB similar to that of the HIV-1 gp41 native hexameric structure, despite mutation of approximately half of the original HR1 sequence or even alteration of the orientation of one of the chains within the native parallel HR1 trimer.[20,21]

Structural analysis of complexes formed between HIV-1-neutralizing HR2 peptides and a synthetic HR1 peptide, i.e., N36, is a constant reminder of the hyperplasticity of the HIV-1 gp41 6-HB structure (Figure 1B,C). For instance, the successfully engineered SC34EK obtained from introducing salt bridges at the solvent-exposed sites of the native C34 sequence still formed stable 6-HB with N36.[22] Apart from solvent-accessible sites, Zheng et al. found that 6-HB structures also allow engineering on the buried binding interface of HR2 helices.[23] Also binding to the gp41 HR1 region to form a typical 6-HB, an artificial α-helical peptide with non-native protein sequence, denoted AP2, was even engineered on the basis of the *ab initio* design of both solvent-exposed residues and amino acids comprising the buried binding interface of

HR2 helices.[24] These studies perfectly demonstrated that the folding properties of the HIV-1 gp41 hexameric coiled-coil assembly were not strictly dependent on matching amino acid sequences between the interacting HR1 and HR2 peptide partners. Rather, the HR1 helical trimers and C-terminal helices could adjust their conformations to each other and adapt folding in a manner sufficient to maintain specific coiled-coil interaction between the two heptad repeats of HIV-1 gp41. This observation implies that the gp41 HR2 helix in the 6-HB fusion core of HIV-1 could even be replaced by other HR2 helices prevalent in viral envelopes, such as those from coronaviruses.

Carrying this notion forward, we envisioned a construct that can take advantage of the common features underlying the folding of class I fusion proteins in the membrane fusion process and the adaptability of the HIV-1 gp41 hexameric coiled-coil fusion complex. Accordingly, we herein report that HIV-1 HR1 trimer inhibitors could cross-bind MERS-CoV and HCoV-OC43 spike protein HR2 regions, thus effectively inhibiting HIV-1, MERS-CoV, and HCoV-OC43 infection. Furthermore, this helical trimer also inhibited SARS-CoV-2 S protein-mediated cell−cell fusion and SARS-CoV-2 pseudovirus efficiently. This study demonstrates that the N-helical trimer isolated from HIV-1 can be further developed as potent

Table 1. Anti-HIV-1 Activity and Cytotoxicity of Peptides[a]

	IC$_{50}$ (nM)					
compound	cell−cell fusion	entry (JRFL)[b]	entry (HIV_25710-2)[b]	infection (BaL)[c]	infection (IIIB)[c]	CC$_{50}$ (μM)[d]
N3G	6.58 ± 1.13	5.48 ± 0.86	5.80 ± 0.97	10.1 ± 1.68	4.77 ± 0.65	>10
N1G	472 ± 1.11	353 ± 112	298 ± 95.0	176 ± 63.2	18.5 ± 6.26	>10
N3HR	>2000	>2000	>2000	>2000	>2000	>10
T20	24.0 ± 1.35	7.86 ± 2.91	11.5 ± 1.70	1.58 ± 0.27	17.8 ± 4.34	>10

[a]Data were derived from the results of three independent experiments and are expressed as the mean ± standard deviation. [b]Inhibition of HIV pseudoviruses with different subtypes. [c]Inhibition of HIV-1 laboratory-adapted strains with different tropisms. [d]Cytotoxicity to MT-2 cells used for testing HIV-1 IIIB infection.

therapeutics against human coronavirus. Moreover, it provides a novel conceptual foundation for the discovery of broad-spectrum antivirals targeting viral entry based on the similarity of superhelical structural motifs found in class I fusion proteins.

DESIGN

We designed trimeric coiled-coil constructs that mimic the inner core of postfusion gp41, taking advantage of our previously established α-helical trimer recapitulation methodology,[19] which is based on the N36/C34 6-HB crystal structure [Protein Data Bank (PDB) entry 1AIK].[25,26] In terms of primary sequence, a coiled-coil domain exhibits a characteristic seven-residue repeat (heptad), usually denoted as $(abcdefg)_n$. The original N36/C34 6-HB contained three HR1 segments spanning HIV-1$_{HXB2}$ residues Ser546−Leu581, both at the outside b positions. As a template, we generated peptide N37 by appending an Ile residue onto the N-terminus of N36 at position a to direct trimer formation (Figure 2A).[27] We engineered the mimetic of the gp41 HR1 helical trimer, designated N3G, on the basis of the N37 sequence and the use of combined strategies, including isoleucine substitution at the a−d sites in the second heptad,[28] intrahelical salt-bridge introduction in the first and third heptad,[27] such as Glu546−Lys550 (i, $i + 4$), Glu547−Lys550 (i, $i + 3$), and Glu560−Lys564 (i, $i + 4$), and intermolecular isopeptide bond formation between the seventh residue Lys and the 12th residue Glu in the adjacent N helix (Figure 2B).[29] Both Asn residues in the second heptad were mutated with His residues to facilitate interchain acyl transfer reaction.[30] To determine the effect of coiled-coil superstructures on antiviral potency, the isopeptide linkage in N3G was replaced with interhelical Glu−Lys ion pair interactions that yielded monomeric peptide N1G. Recently, we described isopeptide bridge-tethered *de novo* coiled-coil trimers, (3HR)$_3$, with three copies of heptad repeat sequence I$_a$Q$_b$Q$_c$I$_d$E$_e$Q$_f$R$_g$.[18] Crystallographic studies have shown that each of the grooves on the gp41 NHR trimer contained a deep pocket that is formed by a cluster of hydrophobic residues in the C-terminal region of N helices (amino acids 565−581).[11] This hydrophobic pocket region of gp41 is known as a hot spot, which is important for the protein−protein interaction between HR1 and HR2. Considering their critical role for the viral 6-HB fusion core stabilization and membrane fusion, the original HR1 trimer mimetic sequences were replaced with *de novo* peptides to explore whether the anti-HIV-1/coronavirus activity was correlated with only the trimeric coiled-coil structure. The partial replacement of the original HR1 trimer mimetic sequences from Ile559 to Arg579 with three repeating IQQIEQR heptads per chain led to N3HR.

RESULTS

Antiviral Activity against HIV-1. First, N3G was tested for its ability to inhibit HIV-1 fusion with its target cell using our previously developed HIV-1 Env-mediated cell−cell fusion assay. As shown in Table 1, N3G could effectively inhibit HIV-1 Env-mediated cell−cell fusion with a half-maximal inhibitory concentration (IC$_{50}$) of 6.58 nM. The use of interstrand ionic interactions in place of isopeptide bonds within N3G led to a 71-fold lower potency. Furthermore, N3HR was devoid of antiviral activity at concentrations of ≤2 μM. Consistent with cell−cell fusion assay results, N3G also strongly inhibited infection by two pseudotyped HIV strains, JRFL (subtype B) and HIV_25710-2 (subtype C), with IC$_{50}$ values of 5.48 and 5.80 nM, respectively. Prominently, N3G exhibited potent inhibitory activity against laboratory-adapted subtype B strain HIV-1$_{BaL}$ that uses co-receptor CCR5 and HIV-1$_{IIIB}$ that uses CXCR4. In contrast, N1G showed significantly decreased anti-HIV-1 activity. Meanwhile, N3HR could not inhibit HIV-1 IIIB or BaL infection at concentrations of ≤2 μM. The selectivity index (SI) of N3G is >2096 (SI = CC$_{50}$/IC$_{50}$ for blocking HIV-1$_{IIIB}$ infection). These results suggest that this mimetic of the gp41 NHR triple helix is a potent inhibitor of HIV-1.

Antiviral Activity against MERS-CoV. We next tested the inhibitory activity of the HIV-1 gp41 NHR coiled-coil mimetic on MERS-CoV S protein-mediated cell−cell fusion and pseudotyped MERS-CoV infection. Notably, compound N3G strongly inhibited cell−cell fusion with an IC$_{50}$ value of 0.34 μM, similar to that of the most active MERS-CoV fusion inhibitor so far named, HR2P-M2, which was derived from the MERS-CoV fusion protein (Table 2).[31] More promisingly, at concentrations of <50 μM, N3G did not exhibit significant cytotoxicity to the target Huh-7 cells, resulting in a high SI value of >147 (SI = CC$_{50}$/IC$_{50}$ for blocking cell−cell fusion). In contrast, removal of the isopeptide linkages markedly

Table 2. Anti-MERS-CoV Activity and Cytotoxicity of Peptides[a]

	IC$_{50}$ (μM)		
compound	MERS-CoV S protein-mediated cell−cell fusion	infection by pseudovirus expressing S protein of MERS-CoV	CC$_{50}$ (μM)[b]
N3G	0.34 ± 0.12	0.25 ± 0.11	>50
N1G	>20	>20	ND[c]
N3HR	>20	>20	ND[c]
HR2P-M2	0.85 ± 0.17	0.45 ± 0.07	>50

[a]Data were derived from the results of three independent experiments and are expressed as the mean ± standard deviation. [b]Cytotoxicity to Huh-7 cells. [c]Not determined.
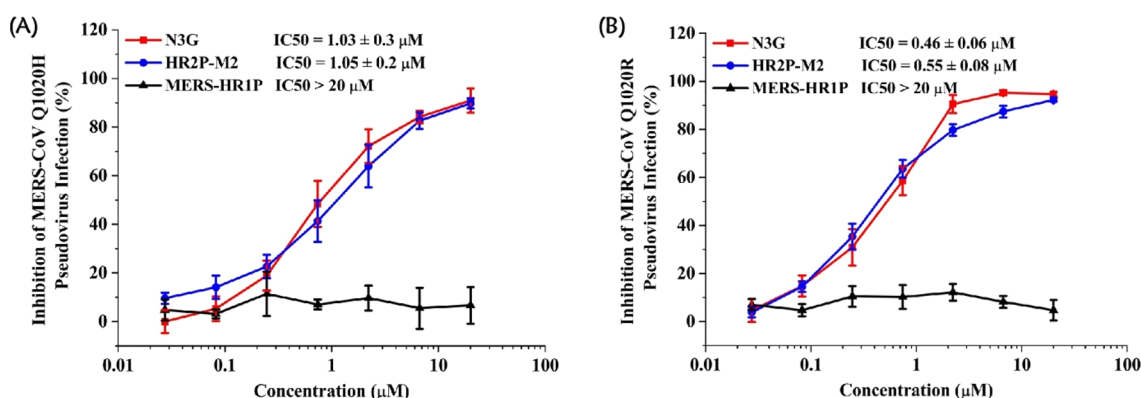
Figure 3. Inhibitory activity of N3G peptide on infection by pseudoviruses expressing MERS-CoV S protein with the (A) Q1020H or (B) Q1020R mutation. MERS-CoV HR1-peptide HR1P was used as a negative control. Each sample was tested in triplicate, and the experiment was repeated twice. Data from a representative experiment are shown as means with the standard deviation.

reduced anti-MERS-CoV activity, resulting in no inhibition of N1G on MERS-CoV infection at concentrations of ≤20 μM. Similar to HIV-1, no anti-MERS-CoV activity was observed with the N3HR trimer. We further tested the inhibitory activity of these HIV-1 NHR-derived peptides on MERS-CoV pseudovirus infection. Consistent with the aforementioned observation in the cell−cell fusion assay, the covalently stabilized coiled coil could inhibit the entry of MERS-CoV in a dose-dependent manner with IC_{50} values in the low micromolar range. On the basis of the epidemiology of MERS-CoV, amino acid mutation Q1020H or Q1020R in the HR1 region is under strong positive selection.[32−34] Strikingly, neither Q1020H nor Q1020R substitution rendered resistance to N3G, indicating its broad-spectrum anti-MERS-CoV potential (Figure 3). Highly encouraged by the *in vitro* MERS-CoV inhibitory data, we sought to observe the *ex vivo* anti-MERS-CoV efficacy of N3G in a mouse model as described recently. HR2P-M2 was also tested as a control. Each peptide was intravenously injected into three BALB/c mice, and serum was collected after 2 min, 20 min, 1 h, 3 h, 7 h, and 12 h. The serum samples from pre- or postadministered mice were tested for their pharmacological kinetics that were reflective of both *in vivo* therapeutic efficacy and pharmaco-kinetic behavior of peptide inhibitors.[35−37] As shown in Figure 4, the peak serum level was observed in the initial sample obtained 2 min after dosing with a 359-fold dilution for N3G and a 348-fold dilution for HR2P-M2. The anti-MERS-CoV activity of serum from mice treated with HR2P-M2 sharply decreased 3 h postinfection, showing serum dilutions of 42-fold, whereas serum samples from mice treated with N3G still exhibited potent inhibitory activity with a serum dilution of 116-fold 3 h after injection. These results suggested that N3G retained its *ex vivo* anti-MERS-CoV activity in mouse blood circulation for at least 3 h and that it may also exert anti-MERS-CoV activity *in vivo*.

Antiviral Activity against HCoV-OC43. Subsequently, we tested the inhibitory activity of N3G on HCoV-OC43 S protein-mediated cell−cell fusion. Strikingly, N3G inhibited cell fusion with an IC_{50} value of 1.26 μM, whereas N1G and N3HR exhibited no significant inhibitory activity at concentrations of ≤20 μM. Similarly, N3G potently inhibited live HCoV-OC43 infection with an IC_{50} value of 6.62 μM. Meanwhile, N3G was not cytotoxic at 40 μM, which is more than 6 times higher than its IC_{50} for inhibiting infection by OC43 (Table 3).
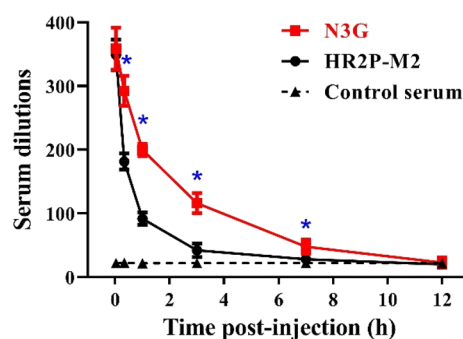

Figure 4. *Ex vivo* anti-MERS-CoV activity of peptides N3G and HR2P-M2. Two groups of three mice ($n = 3$) were administered with each peptide (0.023 mmol/kg) by intravenous injection, and sera were harvested at different time points before or after injection. The antiviral activities of N3G- or HR2P-M2-administered serum or blank mouse serum samples (as a negative control) were tested by the MERS-CoV S protein-mediated cell−cell fusion assay, and serum dilutions required for 50% inhibition of fusion were calculated. An asterisk indicates a significant difference between N3G-treated and HR2P-M2-treated groups (Student's *t* test, $P < 0.05$).

Table 3. Anti-HCoV-OC43 Activity and Cytotoxicity of Peptides[a]

	IC_{50} (μM)		
compound	HCoV-OC43 S protein-mediated cell−cell fusion	infection by live HCoV-OC43	CC_{50} (μM)[b]
N3G	1.26 ± 0.14	6.62 ± 1.78	>40
N1G	>20	>20	>40
N3HR	>20	>20	>40
EK1	0.28 ± 0.06	0.97 ± 0.15	>40

[a]Data were derived from the results of three independent experiments and are expressed as the mean ± standard deviation. [b]Cytotoxicity to RD cells.

Interaction of N3G with Exogenous HIV-1, MERS-CoV, and HCoV-OC43 HR2 Peptides. Early reports showed that HR1 trimers bound to their native HR2 ligand to form stable α-helical complexes, thus blocking virus fusion core formation.[14,17] The native (N)-PAGE method has been widely used to investigate the binding between HR1 and HR2 peptides derived from class I fusion proteins. Therefore, we first performed N-PAGE to confirm the interaction of N3G with target surrogate HR2 peptides from HIV-1, designated
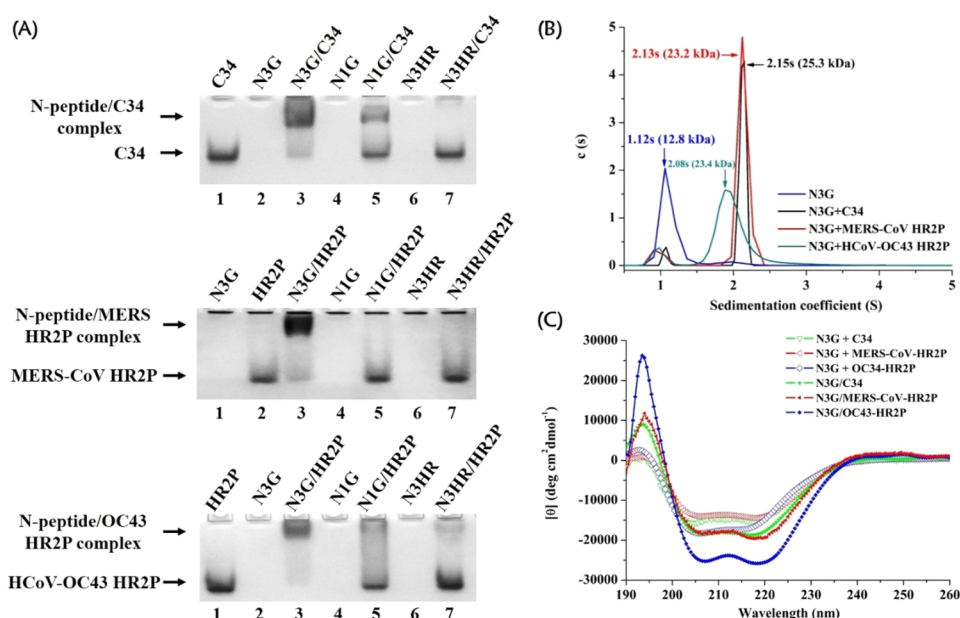
Figure 5. Determination of heterogeneous 6-HB formation. (A) N-PAGE analysis of the interaction between gp41 HR1 mimetics and C34 (top), MERS-CoV-HR2P (middle), or HCoV-OC43-HR2P (bottom). (B) Sedimentation velocity analysis of N3G, the N3G/C34 mixture, the N3G/MERS-CoV-HR2P mixture, and the N3G/HCoV-OC43-HR2P mixture. The buffer was PBS (pH 7.4) for both N3G alone and mixtures. The sedimentation coefficient (s) and molecular mass (kilodaltons) of each peak are indicated. (C) CD spectra of complexes formed between N3G and HR2-derived peptides. The final concentration of each peptide in PBS (pH 7.4) was 15 μM. CD spectra of C34/N3G, MERS-CoV-HR2P/N3G, and HCoV-OC43-HR2P/N3G mixtures (filled symbols) and the theoretical non-interacting spectra of the related isolated peptides [C34 with N3G, MERS-CoV-HR2P with N3G, and HCoV-OC43-HR2P with N3G (empty symbols)] are shown for comparison.
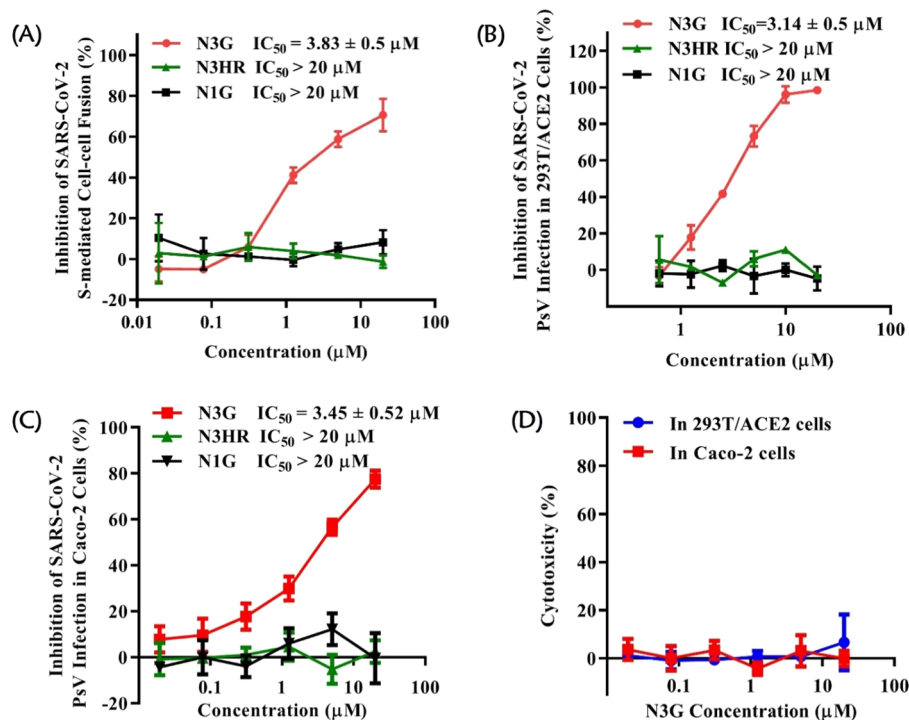

Figure 6. Anti-SARS-CoV-2 activity of N3G, in comparison with N1G and N3HR. (A) Inhibition of N3G on the SARS-CoV-2 S protein-mediated cell−cell fusion. The activities of N3G in inhibiting SARS-CoV-2 in (B) 293T/ACE2 and (C) Caco-2 cells were determined by a single-cycle infection assay. (D) Potential cytotoxicity of the N3G peptide on the 293T/ACE2 and Caco-2 cells that were used as target cells for viral inhibition assays.

C34, MERS-CoV, named MERS-CoV-HR2P, and HCoV-OC43, denoted OC43-HR2P, to form stable complexes.[31,33] As shown in Figure 5A, negatively charged C34 alone migrated rapidly and exhibited a band at the lower position in the gel,

but N3G and N1G showed no band in the N-PAGE gel as a result of its migration up and off the gel owing to its net-positive charges. C34 formed stable oligomeric complexes with N3G as evidenced by the disappearance of the C34 band

concomitant with the appearance of a new band in the upper part of the gel. The mixture of N1G and C34 also showed a band at the upper position in the gel, but with an intensity much lower than that formed by N3G and C34. No new bands were revealed in the lanes where the N3HR trimer and the HIV-1 HR2-derived peptide were loaded. We subsequently assessed the ability of N3G to bind MERS-CoV-HR2P and OC43-HR2P peptides. Strikingly, we saw that N3G could interact with both MERS-CoV-HR2P and OC43-HR2P, forming new bands on the N-PAGE gel. On the contrary, free N1G and N3HR trimer were unable to bind with the MERS-CoV and HCoV-OC43 HR2-derived peptides to form stable complexes. To assess the size of the oligomeric complex formed between N3G and either C34 or HR2P peptides derived from the two HCoVs, we turned to sedimentation velocity analysis (SVA).[17] SVA results showed that the sedimentation coefficients of N3G, the N3G/C34 complex, the N3G/MERS-CoV-HR2P complex, and the N3G/OC43-HR2P complex were 0.77, 2.15, 2.13, and 2.08 s, respectively, corresponding to 12.8, 25.3, 23.2, and 23.4 kDa, respectively, in agreement with the theoretical molecular mass for a N3G trimer (13.2 kDa), a N3G/C34 hexamer consisting of three C34 peptides and a N3G trimer (26.1 kDa), a N3G/MERS-CoV-HR2P hexamer formed by three MERS-CoV-HR2P peptides and a N3G trimer (25.8 kDa), and a N3G/OC43-HR2P hexamer formed by three OC43-HR2P peptides and a N3G trimer (26.2 kDa), respectively (Figure 5B and Table S1). Finally, circular dichroism (CD) spectroscopy was used to investigate the secondary structures of N3G/C34, N3G/MERS-CoV-HR2P, and N3G/OC43-HR2P hexamers. As shown in Figure 5C, CD results showed a distinct α-helical signature for the N3G/C34 complex, as characterized by a maximum signal near 190 nm and double minima at 208 and 222 nm, with an α-helical content of 48.0%. Meanwhile, the CD spectrum of the N3G/MERS-CoV-HR2P and N3G/OC43-HR2P complexes also displayed the characteristic α-helical structures and possessed 53.3% and 73.6% helicity, respectively. Moreover, a difference between the sum of the CD signals of the single peptides and that of the spectrum of their mixture further indicates the interaction between N3G and HR2 peptides derived from HIV-1, MERS-CoV, and HCoV-OC43, which was consistent with the N-PAGE and SVA results. Altogether, we concluded that the mimetic of the HIV-1 N-trimer, N3G, could associate with the HR2 peptide from HIV-1 to form a 6-HB structure that inhibits entry of HIV-1 into the target cell. More interestingly, the N3G peptide could, indeed, cross-interact with MERS-CoV and HCoV-OC43 S protein HR2 regions to form stable helical bundles, thereby exhibiting potent inhibitory activity against MERS-CoV and HCoV-OC43 infection.

N3G Is a Potent Fusion Inhibitor of SARS-CoV-2. Finally, we sought to determine whether the supercoiling structure-based strategy is efficient for the development of SARS-CoV-2 fusion inhibitors. First, we evaluated the fusion inhibitory activity of N3G on cell−cell fusion mediated by S protein of SARS-CoV-2. Encouragingly, N3G showed significant inhibition at a screening concentration of 20 μM, as well as EK1 (Figure S1). As shown in Figure 6A, we further demonstrated that N3G exhibited potent fusion inhibitory activity with an IC$_{50}$ of 3.83 μM. Then, we conducted the single-cycle infection assay to assess the inhibitory potency of N3G against the pseudotyped SARS-CoV-2 entry. Promisingly, consistent with the results from cell−cell fusion assays, the

N3G peptide inhibited SARS-CoV-2 pseudovirus infection in 293T/ACE2 cells with an IC$_{50}$ of 3.14 μM. Meanwhile, N3G could inhibit SARS-CoV-2 pseudovirus infection in Caco-2 cells with an IC$_{50}$ value of 3.45 μM, which is consistent with the result observed in the experiment using 293T/ACE2 cells (Figure 6C). As expected, N1G and N3HR had no inhibitory activity against cell−cell fusion or SARS-CoV-2 pseudovirus. In addition, N3G had no significant cytotoxicity to 293T/ACE2 or Caco-2 cells at concentrations of ≤20 μM (Figure 6D). These results further indicated that the compact trimeric coiled-coil structure of N3G is critical for its anti-human β-coronavirus efficacy. Furthermore, we confirmed an interaction between the N3G and SARS-CoV-2-HR2P by CD mixing experiments. The CD spectrum of the N3G/SARS-CoV-2-HR2P mixture exhibited a total helical content of 78.1% for the system, representing a significant increase over the sum of component spectra (Figure S2).

DISCUSSION

Drug repurposing involves the use of drugs already approved for use in humans. These are then tested for efficacy against emerging and re-emerging viral pathogens.[38] Very recently, this strategy was tested through antiviral drug repurposing in the effort to find a successful treatment for COVID-19 (2019 coronavirus disease).[39] For example, favipiravir (T-705) and remdesivir (GS-5734) have been used in clinics to treat SARS-CoV-2 infection. In 2003, a peptidomimetic of gp41, T20 (brand name, Fuzeon; generic name, enfuvirtide), was approved by the U.S. Food and Drug Administration as the first HIV-1 fusion inhibitor to block HIV-1 viral fusion. During the severe acute respiratory syndrome (SARS) and Middle East respiratory syndrome (MERS) epidemics, researchers explored the potential of T20 against SARS-CoV and MERS-CoV based on similarities of viral fusion between HIV-1 and both coronaviruses. However, T20 had no inhibitory activity on SARS-CoV or MERS-CoV.[31,40] Moreover, HR2 peptides, such as SARS-CoV inhibitor CP-1 and MERS-CoV inhibitor HR2P, were both derived from the coronavirus family, but they failed to exhibit cross-inhibitory activity against MERS-CoV and SARS-CoV infection.[31]

Herein, we demonstrated that peptide mimetics of the trimerized HR1 inner core of HIV-1 could effectively inhibit MERS-CoV, HCoV-OC43, and SARS-CoV-2 infection. This potent dual-entry inhibitor of HIV-1 and coronavirus structurally contains three gp41 HR1 peptides linked through three isopeptide bonds. The designed gp41 HR1 trimeric bundle exhibited potent fusion inhibition similar to that of the HIV-1-specific fusion inhibitor T20 and MERS-CoV-specific fusion inhibitor HR2P-M2. Furthermore, N3G displayed promising inhibitory activity against HCoV-OC43 and SARS-CoV-2 infection. According to CD results, the mimetic of the HIV-1 gp41 N-terminal helical trimer, N3G, showed a helical structure similar with that of free N1G. However, isopeptide bridges afforded a more thermostable trimeric helical conformation (Table S2). The dramatically decreased inhibitory potency of N1G and its weakened target binding proclivity, as observed via N-PAGE, may be explained by its lower structural stability compared to that of the trimeric HR1 oligomer stabilized by isopeptide bonds. This is consistent with previous results showing that tightly associated HR1 helical trimers contribute to their increased antiviral potency.[19] As shown by crystallographic analysis, an HIV-1 gp41 HR2 peptide (e.g., C34 or T20) can interact with an HR1 peptide

(e.g., N36 or N39) to form a stable heterologous 6-HB hexameric coiled coil, in which three C-peptides pack against the inner trimeric coiled coil consisting of N-terminal helices.[26,41] Compared to the target-associated state in a fixed helical conformation, a large decrease in conformational entropy takes place as C peptide inhibitors in their unbound state in a random-coil configuration lose a number of degrees of freedom. In addition, a small increase in binding enthalpy results from the mismatch of residues in inhibitor/cross-target recognition, and this may account for the lack of cross-antiviral activity of C-peptides. Our previous study found that artificial peptides with a stable α-helical conformation in their unbound state could interact with HR1 from both MERS-CoV and influenza A viruses,[8] most likely by the tightening of secondary structure with a resulting decrease in the loss of conformational entropy upon their binding to HR1 targets. In this work, N3G is a supramolecular assembly of α-helical peptides. The relatively low entropy penalty accompanying heterologous 6-HB formation is a consequence of the preorganization of the trimeric coiled-coil conformation favoring its accessibility to the HR2s of HIV-1, MERS-CoV, HCoV-OC43, and SARS-CoV-2 even though the amino acid sequence of the HIV-1 HR2 functional zone is only 31%, 26%, and 38% similar to those of MERS-CoV, OC43, and SARS-CoV-2, respectively (Figure S3). In addition to stable trimeric helical conformations, it is noteworthy that the presence of hydrophobic grooves formed between two adjacent native HR1 helices is also critical for anti-HIV-1/coronavirus activity. Despite the preserved α-helical stability, N3HR misses the binding surface offered by the gp41 HR1 helix trimer and, hence, shows dramatically reduced antiviral activity.

Similar to SARS-CoV-2, SARS-CoV belongs to lineage B betacoronavirus, and both of them have 89.8% sequence similarity in their S protein S2 subunits.[42] Therefore, the N3G peptide was further evaluated against SARS-CoV. We found that N3G inhibited pseudotyped SARS-CoV infection in Caco-2 cells with an IC_{50} of 5.68 ± 2.24 μM, similar to that of EK1 (Figure S4), and exhibited low cytotoxicity to Caco-2 cells, with a CC_{50} of >20 μM (Figure 6D). These results further suggest that the HIV-1 HR1 helical trimer-based peptides have good potential to be developed as broad-spectrum β-coronavirus fusion inhibitors.

In the native state of the fusion protein, the S1 subunit encapsulates the S2 subunit and most of the S1 subunit is exposed. Consequently, the naturally occurring mutations in coronavirus S protein under the pressure of host immunity mainly occur in S1 and RBD. For instance, one of the emerging SARS-CoV-2 variants, South African isolate, harbors three amino acid substitutions in the RBD domain at positions 501, 484, and 417.[43] On the contrary, the S2 subunit, including the HR1 and HR2 region, is highly conserved because of its instantaneous exposure in the fusogenic conformational rearrangement associated with membrane fusion. HR1 involved in membrane fusion is an attractive target for the development of broad-spectrum coronavirus fusion inhibitors.[2] Very recently, we reported several peptide-based pan-coronavirus fusion inhibitors, such as EK1 and EK1C4, which could effectively inhibit infection of divergent HCoVs by targeting the HR1 domain. Previous studies demonstrated that viral resistance to fusion inhibitors is mediated by mutations primarily located at the inhibitor-binding sites.[11] Therefore, the HR2 domain is considered as a new conserved

target for the development of broad-spectrum anticoronavirus agents.

Currently, epidemic viral diseases pose a serious threat to global public health and social stability. In 2018, the World Health Organization (WHO) established a list of prioritized diseases, including SARS, MERS, and an international epidemic caused by an unknown pathogen named Disease X that would be highly transmissible among humans. The availability of a broad-spectrum class of antiviral agents is, therefore, important for the prevention and control of emerging and re-emerging viral pathogens. Membrane fusion is the key step for enveloped virus entry. In this process, a hexameric coiled-coil fusion complex promotes the entry of class I enveloped viruses into host cells, and this α-helix-mediated protein−protein interaction (PPI) has been considered as an optimal target for developing broad-spectrum fusion inhibitor-based drugs. Because of the pivotal roles of PPIs with α-helical components in biological processes, several structural characterizations have allowed a good understanding of structure- and function-related sequence information for this superhelical protein structural motif.[18,29] Within a typical six-helix coiled-coil bundle in viral membrane fusion proteins, residues at the e and g positions of the helical wheels of the HR1 trimers, which are generally hydrophobic, face toward the residues at the a and d positions of the HR2 helical wheels and are largely buried. Therefore, on the basis of the N3G triple-helical scaffold and the established rule of thumb for tuning coiled-coil interactions, further optimization focused on those e and g binding sites in the HR1 helical wheel could lay the groundwork for the development of new inhibitors that can manipulate a broader range of virus−host fusion.

In summary, we have constructed a HIV-1 gp41 prehairpin intermediate mimic as an effective inhibitor of HIV-1, MERS-CoV, HCoV-OC43, and SARS-CoV-2 entry. Extensive data from efficacy evaluation and antiviral mechanistic investigation validate this construct for having good potential as a viral entry inhibitor candidate for future study. The peptides were designed on the basis of the coiled-coil nature of class I fusion protein HR1−HR2 interaction. In a reversal of traditional primary structure-specific design, our study established a novel helical tertiary fold-based paradigm that provides a fresh perspective for viral fusion inhibitor discovery, thus promising timely and effective novel therapies against the increasing number of emerging and re-emerging pathogens. Furthermore, these supercoiled mimetics may inspire the construction of other broad-spectrum antivirals.

■ EXPERIMENTAL SECTION

Peptide Synthesis. All peptides were prepared with a CS Bio Co. peptide synthesizer. The synthesis technique is based on a standard solid-phase Fmoc chemistry protocol. Rink-Amide resin (Nankai Hecheng S&T Co. Ltd., Tianjin, China) with a sample load of 0.44 mmol/g was used. All protected amino acids used were purchased from GL Biochem Ltd. (Shanghai, China). Fmoc-L-glutamic acid O-allyl ester [Fmoc-Glu(OAll)-OH] was used in the thioester-modified site to form isopeptide bonds. In brief, 0.2 M HBTU and 0.2 M HOBt in DMF were added. The former was employed as a coupling reagent, and the latter was used to prevent racemization. To activate the carboxyl group of the amino acids, 2 M DIEA in DMF was used. A mixture of 20% piperidine in DMF was used as a deprotection reagent to remove the Fmoc protecting group. DMF (2×2 min) and DCM (2×2 min) were used to wash the resin after deprotection and coupling. The C-terminus of the peptide taken from the synthesizer was aminated, providing the free amino group at the N-terminus.

Next, an acetic acid anhydride/DIEA mixture [1:1 (v/v)] (2 × 30 min) was added to the resin as the acetylation reagent. For *O*-allyl group removal, 1 equiv of tetrakis(triphenylphosphine)palladium, 10 equiv of 5,5-dimethyl-1,3-cyclohexanedione, as the scavenger, in 5 mL of ultradry DMF, and 5 mL of ultradry THF were added to the resin. A flow of nitrogen was used to avoid contact with air, and the reaction vessel was wrapped in tin foil to protect it from light. The *O*-allyl protecting group was removed after the mixture had been stirred for 6 h. Then the resin was washed with 0.5% sodium diethyldithiocarbamate trihydrate in DMF (5 × 3 min), DMF (2 × 2 min), and DCM (2 × 2 min), and the solvents were removed by draining. 1-Ethyl-3-(3-dimethylaminopropyl)carbodiimide hydrochloride (1 equiv) and HOBt (1.5 equiv) were added to the resin, followed by 4 equiv of benzyl mercaptan, which was used to complete thioester formation. A TFA/anisole/*m*-cresol/water mixture [17:1:1:1 (v/v/v/v)] was used to cleave peptides from the resin. Then a large amount of anhydrous diethyl ether was added to give a white precipitate. The precipitate was dissolved in acetonitrile and water. For isopeptide bond formation, the purified thioester peptide was dissolved in a H_2O/acetonitrile/PBS mixture [5:2:3 (v/v/v), 1×, pH 7.4], stirred at 37 °C for approximately 24 h, and monitored by analytical reverse-phase (RP) HPLC. All lyophilized crude peptides were purified by RP-HPLC (Shimadzu preparative HPLC system), and the purity of each peptide was confirmed to be ≥95% by analytical RP-HPLC (Shimadzu analytical HPLC system). Detailed information is provided in Tables S3 and S4. The molecular weight of the peptides was characterized by MALDI-TOF MS (Autoflex III, Bruker Daltonics Inc., Billerica, MA).

HIV-1 Env-Mediated Cell−Cell Fusion Assay. The HIV-1 Env-mediated cell−cell fusion assay was performed according to a previous report.[36] Fluorescent reagent Calcein AM was used to label H9/HIV-1 IIIB cells. Briefly, 2.5 μL of Calcein AM was used to dye 2 × 10^5 H9/HIV-1 IIIB cells. After being labeled at 37 °C for 30 min, the cells were washed with PBS twice and resuspended with fresh RPMI 1640 containing 10% FBS. Then, 50 μL of diluted peptides and 50 μL of a mixture of 2 × 10^5 H9/HIV-1 IIIB cells/mL were added to a 96-well cell culture plate and incubated at 37 °C for 30 min. Following that, 1 × 10^5 MT-2 cells were added to the mixture and cultured at 37 °C for 2 h. The fused cells were counted under an inverted fluorescence microscope. The IC_{50} values were calculated using CalcuSyn software.[44]

Neutralization of HIV-1 Pseudovirus. The HIV-1 pseudovirus neutralization assay was performed according to a previous study.[45] First, 1 × 10^4 U87 CD4+ CCR5+ cells were seeded into 96-well plates and cultured at 37 °C with 5% CO_2 for 12 h. Then, peptides were diluted and mixed with different subtype HIV-1 pseudoviruses. After incubation at 37 °C for 30 min, the virus/drug mixtures were transferred to cells and replaced with culture medium 12 h postinfection. Forty-eight hours later, the cells were lysed using Cell Culture Lysis Reagent (Promega, Madison, WI), and the luminescence was detected by using the Luciferase Assay System (Promega).

Inhibition of HIV-1 Infection. The inhibitory activities of peptides against laboratory-adapted HIV-1 IIIB (X4) and Bal (R5) were determined as previously described.[45] Briefly, peptides were diluted with FBS-free RPMI 1640 in a 96-well cell culture plate and mixed with 100 TCID50 HIV-1 IIIB or Bal. Then, 10^4 MT-2 cells or CEMx174 5.25 M7 cells were added and cultured at 37 °C overnight. The supernatants were replaced with fresh RPMI 1640 containing 10% FBS. After an additional 3 days for MT-2 cells and 6 days for CEMx174 5.25 M7 cells, the supernatants were collected and lysed with 5% Triton X-100. The P24 antigen was detected using an enzyme-linked immunosorbent assay. The IC_{50} values were calculated using CalcuSyn software.[44]

MERS-CoV S Protein-Mediated Cell−Cell Fusion Assay. The target cells were Huh-7 cells expressing the MERS-CoV receptor dipeptidyl peptidase 4. The effector cells were 293T/MERS/enhanced GFP protein (EGFP) cells. The 293T/MERS/EGFP cells were transfected with a plasmid containing the MERS-CoV S protein gene and the EGFP gene. The 293T/EGFP cells expressing only

EGFP were employed as negative control cells. Huh-7 cells were plated in 96-well plates (5 × 10^4 cells/well) at 37 °C for 5 h. Then, 293T/MERS/EGFP cells or 293T/EGFP cells (1 × 10^4 cells/well) with or without serially diluted peptide were added. After being co-cultured at 37 °C for 2 h, the fused and unfused cells were counted under an inverted fluorescence microscope (Nikon Eclipse Ti-S).

Inhibition of Pseudotyped MERS-CoV Infection. Briefly, the serially diluted tested peptides were added to a 96-well plate and incubated with MERS pseudovirus for 30 min at 37 °C. Then, the pseudovirus/peptide mixture was added to the Huh-7 cells. Cultures were re-fed with fresh medium 12 h postinfection and incubated for an additional 48 h at 37 °C. Fluorescence was determined using a luciferase kit (Promega) and an Ultra 384 luminometer (Tecan).

***Ex Vivo* Anti-MERS-CoV Activity.** Animals were treated in accordance with the Animal Welfare Act and the "Guide for the Care and Use of Laboratory Animals" (NIH Publication 86-23, revised 1985). Briefly, 0.023 mmol/kg of a peptide in PBS (1×, pH 7.4) was administered intravenously to three male BALB/c mice (8 weeks of age). Blood samples were collected at 0 min, 2 min, 20 min, 1 h, 3 h, 7 h, and 12 h and immediately centrifuged to separate the plasma fractions. The mouse serum samples obtained were stored at −20 °C until they were analyzed. Anti-MERS-CoV activities of the mouse serum samples were determined in the same way as that described above. The highest fold dilution of serum causing 50% inhibition of MERS-CoV S protein-mediated cell−cell fusion was calculated.

Inhibition of HCoV-OC43 Spike Protein-Mediated Cell−Cell Fusion. Briefly, HEK293T cells were transfected with plasmid pAAV-IRES-GFP-OC43-S. Thirty-six hours later, HEK293T cells co-expressing EGFP and OC43 spike protein were harvested and co-incubated with diluted peptides at 37 °C for 30 min. Then, 293T cells were transferred and co-incubated with Huh-7 cells in the presence of trypsin for 24 h. The inhibition rate was calculated according to the numbers of fused and unfused cells.

Inhibition of HCoV-OC43 Replication *in Vitro*. The inhibitory activity of peptides against HCoV-OC43 replication in the RD cell line was measured as previously reported.[3] Diluted peptides and HCoV-OC43 (100 $TCID_{50}$) were incubated at 37 °C. After 30 min, mixed solutions containing diluted peptides and HCoV-OC43 were added to RD cells in a 96-well plate. After 3 days, the cytopathic effect was measured with a Cell Counting Kit-8 (CCK-8) assay.

Inhibition of SARS-CoV-2 S-Mediated Cell−Cell Fusion. According to the previous description, the SARS-CoV-2 S protein-mediated cell−cell fusion model was established.[42] Briefly, the expression plasmid carrying SARS-CoV-2 S protein and EGFP (pAAV-SARS-CoV-2-S) was transfected into 293T to produce effector cells (293T/S/EGFP) for cell−cell fusion, and the empty expression plasmid (pAAV-IRES-EGFP) was used as a negative control (293T/EGFP). After transfection for 48 h, effector cells were collected in Dulbecco's modified Eagle's medium (DMEM) without FBS for cell−cell fusion. Six to eight hours before cell−cell fusion, the target cells (ACE2-293T) were plated at a density of 10^5 cells/well in a 96-well plate with complete medium. Then the supernatant was removed, and 10^4 effector cells were added to each well and incubated at 37 °C for 24 h. Finally, the cell−cell fusion was observed with a fluorescence microscope. To assess the inhibitory activity of peptides, gradient dilutions of peptides were added, and the cell−cell fusion was observed after co-incubation for 24 h. The percentage inhibition of cell−cell fusion was calculated according to the numbers of fused and unfused cells.

Inhibition of Pseudotyped SARS-CoV-2 Infection. To detect the inhibitory activity of peptides on infection of pseudotyped SARS-CoV-2, target cells (ACE2−293T) were plated at a density of 10^4 cells/well in a 96-well plate 12 h before infection. Diluted pseudotyped SARS-CoV-2 was mixed with peptides that were series diluted with DMEM without FBS and incubated at 37 °C for 30 min. The mixture was transferred to the ACE2-293T cells and incubated for 12 h. After that, the supernatant was replaced with complete medium and incubation continued for 48 h. Luciferase activity was analyzed by using the Luciferase Assay System (Promega), which

refers to the amount of pseudotyped SARS-CoV-2 infecting target cells.[42]

Cytotoxicity Assays. Briefly, 100 μL of the cell suspension (1 × 10^5 cells/mL) was added to each well of a 96-well culture plate and incubated at 37 °C in 5% CO$_2$ for 12 h. Next, 5 μL of a serially diluted peptide solution was added. At the same time, a blank control group without peptide and a positive control group with 5 μL of 10% Triton X-100 were cultured for 48 h under 5% CO$_2$ at 37 °C. To each well was added 10 μL of the Cell Counting Kit-8 solution, and the plate was incubated for an additional 2 h. The absorbance at 450 nm was determined by a microplate reader.

CD Spectroscopy. The N-peptides and C34 or HR2P were dissolved in ddH$_2$O and PBS (1×, pH 7.4), respectively, at a concentration of 15 μM. The equimolar mixtures were incubated at 37 °C for 30 min at a final concentration of 15 μM. The CD spectra were recorded on a MOS-450 system (BioLogic, Claix, France) under the following conditions: room temperature; wavelength, 190−260 nm; resolution, 0.1 nm; path length, 0.1 cm; response time, 4.0 s; and scanning speed, 50 nm/min. The obtained results were processed to obtain the mean residue ellipticity. A mean residue ellipticity $[\theta]$ of −33000 deg cm^2 dmol^{-1} at a wavelength of 222 nm was considered to be 100% α-helicity. Thermal denaturation was monitored at 222 nm by the change in ellipticity by applying a thermal gradient of 5 °C/min from 20 to 90 °C.

N-PAGE. Peptides at a final concentration of 50 μM, including the N- and C-terminal free peptides, as well as their equimolar mixtures, were dissolved in PBS (1×, pH 7.4) and incubated at 37 °C for 30 min. After the peptides mentioned above had been mixed with Tris-glycine native sample buffer (Bio-Rad, Hercules, CA) in a 1:1 ratio, the samples were loaded (20 μL in each well) onto 10% Tris-glycine gels. Gel electrophoresis was performed under a constant voltage of 120 V at room temperature for 4 h. The obtained gel was then stained with Coomassie Blue R250. The images were taken by the ChampGel 6000 Imaging System (Sage Creation Ltd., Beijing, China).

Sedimentation Velocity Analysis (SVA). SVA was performed using a Proteomelab XL-A/XL-I analytical ultracentrifuge (Beckman Coulter, Fullerton, CA) equipped with a three-channel cell and an An-60 Ti rotor. All samples were prepared at a final concentration of 150 μM in PBS (1×, pH 7.4). The N3G/HR2 peptide mixtures were incubated at 37 °C for 30 min and initially scanned at 3000 rpm for 10 min. Data were obtained at a wavelength of 280 nm after centrifugation at 60000 rpm and 20 °C for 7 h. Weight-average molecular weights were calculated and fitted by processing with SEDFIT.

■ ASSOCIATED CONTENT

Ⓢ Supporting Information

The Supporting Information is available free of charge at https://pubs.acs.org/doi/10.1021/acs.jmedchem.1c00258.

> Summary of the SVA results; biophysical properties of the designed peptides; HPLC method used for the purification of peptide compounds; HPLC method used for the analysis of peptide compounds; evidence that both N3G and EK1 are effective against SARS-CoV-2 infection; CD spectra of the complex formed between N3G and SARS-CoV-2 HR2P; sequence similarity between the HR2 domain of MERS-CoV, OC43, or SARS-CoV-2 and that of HIV-1; inhibitory activity of peptides on pseudotyped SARS-CoV infection; and MALDI-TOF-MS and analytical HPLC of designed peptides (PDF)

> Molecular formula strings of all compounds (CSV)

■ AUTHOR INFORMATION

Corresponding Authors

Shibo Jiang − *Key Laboratory of Medical Molecular Virology (MOE/NHC/CAMS), School of Basic Medical Sciences & Shanghai Public Health Clinical Center, Fudan University, Shanghai 200032, China; Lindsley F. Kimball Research Institute, New York Blood Center, New York 10065, United States;* ⓞ orcid.org/0000-0001-8283-7135; Phone: 86-21-5423-7673; Email: shibojiang@fudan.edu.cn; Fax: 86-21-5423-7465

Keliang Liu − *State Key Laboratory of Toxicology and Medical Countermeasures, Beijing Institute of Pharmacology and Toxicology, Beijing 100850, China;* ⓞ orcid.org/0000-0002-9133-377X; Phone: 86-10-6693-0640; Email: keliangliu55@126.com; Fax: 86-10-6821-1656

Fei Yu − *Hebei Center for Wildlife Health, College of Life Sciences, Hebei Agricultural University, Baoding 071001, China;* Phone: 86-312-7528935; Email: shmyf@hebau.edu.cn

Qian Wang − *Key Laboratory of Medical Molecular Virology (MOE/NHC/CAMS), School of Basic Medical Sciences & Shanghai Public Health Clinical Center, Fudan University, Shanghai 200032, China;* Phone: 86-21-5423-7671; Email: wang_qian@fudan.edu.cn; Fax: 86-21-5423-7465

Authors

Chao Wang − *State Key Laboratory of Toxicology and Medical Countermeasures, Beijing Institute of Pharmacology and Toxicology, Beijing 100850, China*

Shuai Xia − *Key Laboratory of Medical Molecular Virology (MOE/NHC/CAMS), School of Basic Medical Sciences & Shanghai Public Health Clinical Center, Fudan University, Shanghai 200032, China*

Xinling Wang − *Key Laboratory of Medical Molecular Virology (MOE/NHC/CAMS), School of Basic Medical Sciences & Shanghai Public Health Clinical Center, Fudan University, Shanghai 200032, China*

Yue Li − *State Key Laboratory of Toxicology and Medical Countermeasures, Beijing Institute of Pharmacology and Toxicology, Beijing 100850, China*

Huan Wang − *State Key Laboratory of Toxicology and Medical Countermeasures, Beijing Institute of Pharmacology and Toxicology, Beijing 100850, China*

Rong Xiang − *Hebei Center for Wildlife Health, College of Life Sciences, Hebei Agricultural University, Baoding 071001, China*

Qinwen Jiang − *Key Laboratory of Structure-based Drug Design & Discovery of the Ministry of Education, Shenyang Pharmaceutical University, Shenyang 110016, China*

Qiaoshuai Lan − *Key Laboratory of Medical Molecular Virology (MOE/NHC/CAMS), School of Basic Medical Sciences & Shanghai Public Health Clinical Center, Fudan University, Shanghai 200032, China*

Ruiying Liang − *Hebei Center for Wildlife Health, College of Life Sciences, Hebei Agricultural University, Baoding 071001, China*

Qing Li − *State Key Laboratory of Toxicology and Medical Countermeasures, Beijing Institute of Pharmacology and Toxicology, Beijing 100850, China*

Shanshan Huo − *Hebei Center for Wildlife Health, College of Life Sciences, Hebei Agricultural University, Baoding 071001, China*

Lu Lu − *Key Laboratory of Medical Molecular Virology (MOE/NHC/CAMS), School of Basic Medical Sciences & Shanghai Public Health Clinical Center, Fudan University, Shanghai 200032, China*

Complete contact information is available at:
https://pubs.acs.org/10.1021/acs.jmedchem.1c00258

Author Contributions

Notes

The authors declare no competing financial interest.

■ ACKNOWLEDGMENTS

■ REFERENCES

(1) World Health Organization. http://www.who.int/emergencies/mers-cov/en (accessed October 2020).

(2) Wang, X.; Xia, S.; Wang, Q.; Xu, W.; Li, W.; Lu, L.; Jiang, S. Broad-spectrum coronavirus fusion inhibitors to combat COVID-19 and other emerging coronavirus diseases. *Int. J. Mol. Sci.* **2020**, *21*, 3843−3859.

(3) Xia, S.; Yan, L.; Xu, W.; Agrawal, A. S.; Algaissi, A.; Tseng, C. K.; Wang, Q.; Du, L.; Tan, W.; Wilson, I. A.; Jiang, S.; Yang, B.; Lu, L. A pan-coronavirus fusion inhibitor targeting the HR1 domain of human coronavirus spike. *Sci. Adv.* **2019**, *5*, eaav4580.

(4) Dimitrov, D. S. Virus entry: molecular mechanisms and biomedical applications. *Nat. Rev. Microbiol.* **2004**, *2*, 109−122.

(5) Harrison, S. C. Viral membrane fusion. *Nat. Struct. Mol. Biol.* **2008**, *15*, 690−698.

(6) Follis, K. E.; York, J.; Nunberg, J. H. Serine-scanning mutagenesis studies of the C-terminal heptad repeats in the SARS coronavirus S glycoprotein highlight the important role of the short helical region. *Virology* **2005**, *341*, 122−129.

(7) Xu, Y.; Zhu, J.; Liu, Y.; Lou, Z.; Yuan, F.; Liu, Y.; Cole, D. K.; Ni, L.; Su, N.; Qin, L.; Li, X.; Bai, Z.; Bell, J. I.; Pang, H.; Tien, P.; Gao, G. F.; Rao, Z. Characterization of the heptad repeat regions, HR1 and HR2, and design of a fusion core structure model of the spike protein from severe acute respiratory syndrome (SARS) coronavirus. *Biochemistry* **2004**, *43*, 14064−14071.

(8) Wang, C.; Zhao, L.; Xia, S.; Zhang, T.; Cao, R.; Liang, G.; Li, Y.; Meng, G.; Wang, W.; Shi, W.; Zhong, W.; Jiang, S.; Liu, K. De novo design of α-helical lipopeptides targeting viral fusion proteins: a promising strategy for relatively broad-spectrum antiviral drug discovery. *J. Med. Chem.* **2018**, *61*, 8734−8745.

(9) Eckert, D. M.; Kim, P. S. Mechanisms of viral membrane fusion and its inhibition. *Annu. Rev. Biochem.* **2001**, *70*, 777−810.

(10) Colman, P. M.; Lawrence, M. C. The structural biology of type I viral membrane fusion. *Nat. Rev. Mol. Cell Biol.* **2003**, *4*, 309−319.

(11) Cai, L.; Jiang, S. Development of peptide and small-molecule HIV-1 fusion inhibitors that target gp41. *ChemMedChem* **2010**, *5*, 1813−1824.

(12) Berkhout, B.; Eggink, D.; Sanders, R. W. Is there a future for antiviral fusion inhibitors? *Curr. Opin. Virol.* **2012**, *2*, 50−59.

(13) Eckert, D. M.; Kim, P. S. Design of potent inhibitors of HIV-1 entry from the gp41 N-peptide region. *Proc. Natl. Acad. Sci. U. S. A.* **2001**, *98*, 11187−11192.

(14) Chen, X.; Lu, L.; Qi, Z.; Lu, H.; Wang, J.; Yu, X.; Chen, Y.; Jiang, S. Novel recombinant engineered gp41 N-terminal heptad repeat trimers and their potential as anti-HIV-1 therapeutics or microbicides. *J. Biol. Chem.* **2010**, *285*, 25506−25515.

(15) Clinton, T. R.; Weinstock, M. T.; Jacobsen, M. T.; Szabo-Fresnais, N.; Pandya, M. J.; Whitby, F. G.; Herbert, A. S.; Prugar, L. I.; McKinnon, R.; Hill, C. P.; Welch, B. D.; Dye, J. M.; Eckert, D. M.; Kay, M. S. Design and characterization of ebolavirus GP prehairpin intermediate mimics as drug targets. *Protein Sci.* **2015**, *24*, 446−463.

(16) Bianchi, E.; Finotto, M.; Ingallinella, P.; Hrin, R.; Carella, A. V.; Hou, X. S.; Schleif, W. A.; Miller, M. D.; Geleziunas, R.; Pessi, A. Covalent stabilization of coiled coils of the HIV gp41 N region yields extremely potent and broad inhibitors of viral infection. *Proc. Natl. Acad. Sci. U. S. A.* **2005**, *102*, 12903−12908.

(17) Tong, P.; Lu, Z.; Chen, X.; Wang, Q.; Yu, F.; Zou, P.; Yu, X.; Li, Y.; Lu, L.; Chen, Y.; Jiang, S. An engineered HIV-1 gp41 trimeric coiled coil with increased stability and anti-HIV-1 activity: implication for developing anti-HIV microbicides. *J. Antimicrob. Chemother.* **2013**, *68*, 2533−2544.

(18) Wang, C.; Lai, W.; Yu, F.; Zhang, T.; Lu, L.; Jiang, X.; Zhang, Z.; Xu, X.; Bai, Y.; Jiang, S.; Liu, K. De novo design of isopeptide bond-tethered triple-stranded coiled coils with exceptional resistance to unfolding and proteolysis: implication for developing antiviral therapeutics. *Chem. Sci.* **2015**, *6*, 6505−6509.

(19) Lai, W.; Wang, C.; Yu, F.; Lu, L.; Wang, Q.; Jiang, X.; Xu, X.; Zhang, T.; Wu, S.; Zheng, X.; Zhang, Z.; Dong, F.; Jiang, S.; Liu, K. An effective strategy for recapitulating N-terminal heptad repeat trimers in enveloped virus surface glycoproteins for therapeutic applications. *Chem. Sci.* **2016**, *7*, 2145−2150.

(20) Dwyer, J. J.; Wilson, K. L.; Martin, K.; Seedorff, J. E.; Hasan, A.; Medinas, R. J.; Davison, D. K.; Feese, M. D.; Richter, H. T.; Kim, H.; Matthews, T. J.; Delmedico, M. K. Design of an engineered N-terminal HIV-1 gp41 trimer with enhanced stability and potency. *Protein Sci.* **2008**, *17*, 633−643.

(21) Crespillo, S.; Camara-Artigas, A.; Casares, S.; Morel, B.; Cobos, E. S.; Mateo, P. L.; Mouz, N.; Martin, C. E.; Roger, M. G.; El Habib, R.; Su, B.; Moog, C.; Conejero-Lara, F. Single-chain protein mimetics of the N-terminal heptad-repeat region of gp41 with potential as anti-HIV-1 drugs. *Proc. Natl. Acad. Sci. U. S. A.* **2014**, *111*, 18207−18212.

(22) Nishikawa, H.; Nakamura, S.; Kodama, E.; Ito, S.; Kajiwara, K.; Izumi, K.; Sakagami, Y.; Oishi, S.; Ohkubo, T.; Kobayashi, Y.; Otaka, A.; Fujii, N.; Matsuoka, M. Electrostatically constrained α-helical peptide inhibits replication of HIV-1 resistant to enfuvirtide. *Int. J. Biochem. Cell Biol.* **2009**, *41*, 891−899.

(23) Zheng, B.; Wang, K.; Lu, L.; Yu, F.; Cheng, M.; Jiang, S.; Liu, K.; Cai, L. Hydrophobic mutations in buried polar residues enhance HIV-1 gp41 N-terminal heptad repeat-C-terminal heptad repeat interactions and C-peptides' anti-HIV activity. *AIDS* **2014**, *28*, 1251−1260.

(24) Zhu, X.; Zhu, Y.; Ye, S.; Wang, Q.; Xu, W.; Su, S.; Sun, Z.; Yu, F.; Liu, Q.; Wang, C.; Zhang, T.; Zhang, Z.; Zhang, X.; Xu, J.; Du, L.; Liu, K.; Lu, L.; Zhang, R.; Jiang, S. Improved pharmacological and structural properties of HIV fusion inhibitor AP3 over enfuvirtide: highlighting advantages of artificial peptide strategy. *Sci. Rep.* **2015**, *5*, 13028.

(25) Lu, M.; Kim, P. S. A trimeric structural subdomain of the HIV-1 transmembrane glycoprotein. *J. Biomol. Struct. Dyn.* **1997**, *15*, 465−471.

(26) Chan, D. C.; Fass, D.; Berger, J. M.; Kim, P. S. Core structure of gp41 from the HIV envelope glycoprotein. *Cell* **1997**, *89*, 263−273.

(27) Apostolovic, B.; Danial, M.; Klok, H. A. Coiled coils: attractive protein folding motifs for the fabrication of self-assembled, responsive and bioactive materials. *Chem. Soc. Rev.* **2010**, *39*, 3541−3575.

(28) Fletcher, J. M.; Boyle, A. L.; Bruning, M.; Bartlett, G. J.; Vincent, T. L.; Zaccai, N. R.; Armstrong, C. T.; Bromley, E. H.; Booth, P. J.; Brady, R. L.; Thomson, A. R.; Woolfson, D. N. A basis set of de novo coiled-coil peptide oligomers for rational protein design and synthetic biology. *ACS Synth. Biol.* **2012**, *1*, 240−250.

(29) Wang, C.; Li, X.; Yu, F.; Lu, L.; Jiang, X.; Xu, X.; Wang, H.; Lai, W.; Zhang, T.; Zhang, Z.; Ye, L.; Jiang, S.; Liu, K. Site-specific isopeptide bridge tethering of chimeric gp41 N-terminal heptad

repeat helical trimers for the treatment of HIV-1 infection. *Sci. Rep.* **2016**, *6*, 32161.

(30) Wilcoxen, K. M.; Leman, L. J.; Weinberger, D. A.; Huang, Z. Z.; Ghadiri, M. R. Biomimetic catalysis of intermodular aminoacyl transfer. *J. Am. Chem. Soc.* **2007**, *129*, 748−749.

(31) Lu, L.; Liu, Q.; Zhu, Y.; Chan, K.; Qin, L.; Li, Y.; Wang, Q.; Chan, J.; Du, L.; Yu, F.; Ma, C.; Ye, S.; Yuen, K.; Zhang, R.; Jiang, S. Structure-based discovery of middle east respiratory syndrome coronavirus fusion inhibitor. *Nat. Commun.* **2014**, *5*, 3067−3078.

(32) Cotten, M.; Watson, S. J.; Zumla, A. I.; Makhdoom, H. Q.; Palser, A. L.; Ong, S. H.; Al Rabeeah, A. A.; Alhakeem, R. F.; Assiri, A.; Al-Tawfiq, J. A.; Albarrak, A.; Barry, M.; Shibl, A.; Alrabiah, F. A.; Hajjar, S.; Balkhy, H. H.; Flemban, H.; Rambaut, A.; Kellam, P.; Memish, Z. A. Spread, circulation, and evolution of the middle east respiratory syndrome coronavirus. *mBio* **2014**, *5*, e01062-13.

(33) Xia, S.; Lan, Q.; Pu, J.; Wang, C.; Liu, Z.; Xu, W.; Wang, Q.; Liu, H.; Jiang, S.; Lu, L. Potent MERS-CoV fusion inhibitory peptides identified from HR2 domain in spike protein of bat coronavirus HKU4. *Viruses* **2019**, *11*, 56.

(34) Wang, C.; Xia, S.; Zhang, P.; Zhang, T.; Wang, W.; Tian, Y.; Meng, G.; Jiang, S.; Liu, K. Discovery of hydrocarbon-stapled short alpha-helical peptides as promising middle east respiratory syndrome coronavirus (MERS-CoV) fusion inhibitors. *J. Med. Chem.* **2018**, *61*, 2018−2026.

(35) Chong, H.; Wu, X.; Su, Y.; He, Y. Development of potent and long-acting HIV-1 fusion inhibitors. *AIDS* **2016**, *30*, 1187−1196.

(36) Su, S.; Ma, Z.; Hua, C.; Li, W.; Lu, L.; Jiang, S. Adding an artificial tail-anchor to a peptide-based HIV-1 fusion inhibitor for improvement of its potency and resistance profile. *Molecules* **2017**, *22*, 1996.

(37) Li, H.; Yu, F.; Xia, S.; Yu, Y.; Wang, Q.; Lv, M.; Wang, Y.; Jiang, S.; Lu, L. Chemically modified human serum albumin potently blocks entry of Ebola pseudoviruses and viruslike particles. *Antimicrob. Agents Chemother.* **2017**, *61*, e02168-16.

(38) Serafin, M.; Bottega, A.; Foletto, V.; da Rosa, T. F.; Hörner, A.; Hörner, R. Drug repositioning is an alternative for the treatment of coronavirus COVID-19. *Int. J. Antimicrob. Agents* **2020**, *55*, 105969.

(39) Zhou, Y.; Hou, Y.; Shen, J.; Huang, Y.; Martin, W.; Cheng, F. Network-based drug repurposing for novel coronavirus 2019-nCoV/SARS-CoV-2. *Cell Discovery* **2020**, *6*, 14.

(40) Veiga, S.; Yuan, Y.; Li, X.; Santos, N.; Liu, G.; Castanho, M. Why are HIV-1 fusion inhibitors not effective against SARS-CoV? *Biochim. Biophys. Acta, Gen. Subj.* **2006**, *1760*, 55−61.

(41) Zhang, X.; Ding, M.; Zhu, Y.; Chong, H.; Cui, S.; He, J.; Wang, X.; He, Y. Structural and functional characterization of HIV-1 cell fusion inhibitor T20. *AIDS* **2019**, *33*, 1−11.

(42) Xia, S.; Liu, M.; Wang, C.; Xu, W.; Lan, Q.; Feng, S.; Qi, F.; Bao, L.; Du, L.; Liu, S.; Qin, C.; Sun, F.; Shi, Z.; Zhu, Y.; Jiang, S.; Lu, L. Inhibition of SARS-CoV-2 (previously 2019-nCoV) infection by a highly potent pan-coronavirus fusion inhibitor targeting its spike protein that harbors a high capacity to mediate membrane fusion. *Cell Res.* **2020**, *30*, 343−355.

(43) Sakharkar, M.; Rappazzo, C. G.; Wieland-Alter, W. F.; Hsieh, C. L.; Wrapp, D.; Esterman, E. S.; Kaku, C. I.; Wec, A. Z.; Geoghegan, J. C.; McLellan, J. S.; Connor, R. I.; Wright, P. F.; Walker, L. M. Prolonged evolution of the human B cell response to SARS-CoV-2 infection. *Sci. Immunol.* **2021**, *6*, eabg6916.

(44) Chou, T. C. Theoretical basis, experimental design, and computerized simulation of synergism and antagonism in drug combination studies. *Pharmacol. Rev.* **2006**, *58*, 621−681.

(45) Su, S.; Zhu, Y.; Ye, S.; Qi, Q.; Xia, S.; Ma, Z.; Yu, F.; Wang, Q.; Zhang, R.; Jiang, S.; Lu, L. Creating an artificial tail anchor as a novel strategy to enhance the potency of peptide-based HIV fusion inhibitors. *J. Virol.* **2017**, *91*, e01445-16.